JACS
JOURNAL OF THE AMERICAN CHEMICAL SOCIETY

Article

pubs.acs.org/JACS

Precursor Triggering Synthesis of Self-Coupled Sulfide Polymorphs with Enhanced Photoelectrochemical Properties

Shi-Kui Han,[†,∥] Chao Gu,[†,∥] Songtao Zhao,[‡,∥] Sen Xu,[‡] Ming Gong,[§] Zhenyu Li,*[,‡] and Shu-Hong Yu*[,†]

[†]Division of Nanomaterials & Chemistry, Hefei National Laboratory for Physical Sciences at the Microscale, Collaborative Innovation Center of Suzhou Nano Science and Technology, CAS Centre for Excellence in Nanoscience, Department of Chemistry, University of Science and Technology of China, Hefei, Anhui 230026, China

[‡]Division of Theoretical and Computational Sciences, Hefei National Laboratory for Physical Sciences at the Microscale, CAS Centre for Excellence and Synergetic Innovation Centre in Quantum Information and Quantum Physics, University of Science and Technology of China, Hefei, Anhui 230026, China

[§]Lab of Mechanical and Material Science, School of Engineering Science, University of Science and Technology of China, Hefei, Anhui 230026, China

Supporting Information

ABSTRACT: Heteronanostructures have attracted intensive attention due to their electronic coupling effects between distinct components. Despite tremendous advances of nanostructure fabrication, combining independent polymorphs by forming heterojunction is still challenging but fascinating, such as copper sulfides ($Cu_{2-x}S$), exhibiting varying band gaps and crystal structures with various stoichiometries. Herein, self-coupled $Cu_{2-x}S$ polymorphs ($Cu_{1.94}S$-CuS) by a facile one-pot chemical transformation route have been reported for the first time. Unprecedentedly, a manganous precursor plays a crucial role in inducing and directing the formation of such a dumbbell-like architecture, which combines 1D $Cu_{1.94}S$ with 2D CuS. During the transformation, Mn^{2+} ions mediate the Cu^{+} ions diffusion and phase conversion process particularly. Furthermore, this self-coupled polymorphic structure exhibits significantly enhanced photoelectrochemical properties compared with the individual $Cu_{1.94}S$ nanocrystals and CuS nanoplates, originating from the unique heterointerfaces constructed by intrinsic band alignment and the enhanced contact between high conductivity hexagonal planes and the working electrode revealed by density functional theory (DFT) calculations. So we anticipate this emerging interfacial charge separation could provide useful hints for applications in optoelectronic devices or photocatalysis.

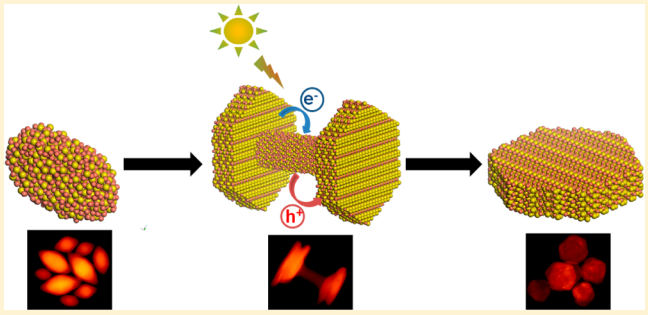

INTRODUCTION

Semiconductor nanocrystals,[1] as an important branch of nanomaterials, have attracted extensive interest from researchers in chemistry, physics, material science and other fields.[2] This is because the chemical and physical properties of semiconductor nanocrystals depend strongly on their size, shape, and crystal structure.[3,4] Recently, as a new class of nanoscale building blocks, heteronanostructures have gained tons of attention due to containing two or more chemically distinct components in one single structure with multifunctionalities or novel properties induced by the heterointerfaces.[5−8] These ideas are representatively demonstrated in semiconductor-metal hybrids as coupling strongly plasmonic effects with photogenerated carrier separation and transport.[9] Pioneering work on semiconductor-metal hybrids with "real metal or alloy", for instance, Au-ZnO,[10] Au−Pt−Fe_3O_4,[11] Ag−Fe@Fe_xO_y,[12] PdPt-Fe_3O_4,[13] PtNi-CdS,[14] ZnS-(CdS/Au)[15] and Ag/Bi-based heteronanostructures,[16] has been systematically studied, while reports on using metallic chalcogenide as the "metal domain" are rare.[17] So it would be a great supplement to nanostructure synthesis and electronic coupling effects if we could fabricate such an interface.

Copper sulfides ($Cu_{2-x}S$), as one of excellent p-type materials due to copper vacancies in the lattice, possess localized surface plasmon resonances (LSPR)[18] and an x-dependent bandgap energy varying from about 1.2 eV for chalcocite ($x = 0$) to 2.0 eV for covellite ($x = 1$) (E_g = 1.2 eV for Cu_2S, 1.5 eV for $Cu_{1.8}S$ and 2.0 eV for CuS), matching extremely well with the solar spectrum.[19] Owing to these unique properties, enormous efforts have been devoted to the synthesis of diverse Cu_2S[20−24] and CuS[25−30] nanocrystals and $Cu_{2-x}S$ based ternary and quaternary structures (e.g., $CuInS_2$ and $CuIn_xGa_{1-x}S_2$).[31] However, current research was mainly focused on single phase of $Cu_{2-x}S$, thus further combining different polymorphs by forming heterojunction will be indeed an exciting rather challenging task in regard to achieving special and robust functionalities.

Received: June 27, 2016
Published: July 26, 2016

DOI: 10.1021/jacs.6b06609
J. Am. Chem. Soc. 2016, 138, 12913−12919

Herein, for the first time we report a facile one-pot chemical transformation route to the synthesis of self-coupled $Cu_{2-x}S$ polymorphs (Or rather, $Cu_{1.94}S$-CuS by further analysis). As the intermediate products of the phase transformation and shape evolution process from monoclinic egg-like $Cu_{1.94}S$ nanocrystals to hexagonal CuS nanoplates mediated by a manganous precursor, the obtained self-coupled $Cu_{2-x}S$ polymorphs are stable and can be isolated. We believe this approach can be a powerful supplement to the general tool bench with introducing foreign ion precursors as potential morphology and phase regulators for nanostructure fabrication.

RESULTS AND DISCUSSION

The sample of self-coupled $Cu_{2-x}S$ polymorphs was synthesized in a 25 mL three-necked flask by using CuCl and $Mn(S_2CNEt_2)_2$ as precursors in oleylamine (OLA) at 125 °C (see detailed information in Experimental Section). Representative scanning and transmission electron microscopy (SEM and TEM) images displayed in Figure 1a and 1b demonstrate

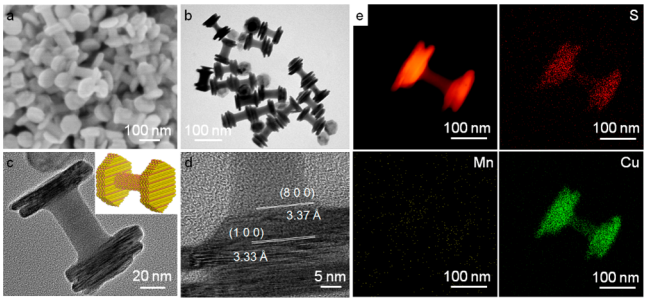

Figure 1. (a) SEM image, (b) TEM image, (c,d) HRTEM images and (e) STEM-EDS elemental mapping images of the self-coupled $Cu_{2-x}S$ polymorphs (inset c is the corresponding crystal structures of the self-coupled $Cu_{2-x}S$ polymorphs. Red ball represents Cu atom and yellow for S atom).

that each structure is dumbbell-like in shape with a length of about 100 nm and a diameter of about 20 nm. The corresponding X-ray diffraction (XRD) pattern is shown in Figure S1, indicating that the sample is composed of crystalline phases of $Cu_{1.94}S$ (JCPDS No. 23−0959, monoclinic, a = 26.897 Å, b = 15.745 Å, c = 13.565 Å) and hexagonal CuS (JCPDS No. 65−3561). Moreover, high-resolution TEM (HRTEM) confirms the orientational relationship between $Cu_{1.94}S$ and CuS components as shown in Figure 1c and 1d. The analysis of the lattice spacing reveals that the (8 0 0) planes (d = 3.37 Å) of $Cu_{1.94}S$ are coincident with the (1 0 0) planes (d = 3.33 Å) of CuS. Further the STEM-EDS elemental mapping was applied to obtain elemental distribution of Cu, Mn and S in the structure. Figure 1e displays that elemental Cu and S are uniformly distributed within the structure, while no presence of elemental Mn is detected. So it is merely composed of elemental Cu and S. In conclusion, we confirmed that the self-coupled $Cu_{2-x}S$ polymorphs are $Cu_{1.94}S$-CuS heteronanostructures.

To determine the exact formation process of the self-coupled $Cu_{2-x}S$ polymorphs, a series of experiments with different reaction time were performed. When the temperature reached 125 °C, it was just egg-like nanocrystals obtained at the beginning which could be indexed as monoclinic $Cu_{1.94}S$ (Figure S2). As shown in Figure 2a, the elemental Mn did not exist in the nanocrystals from the mapping analysis. As the

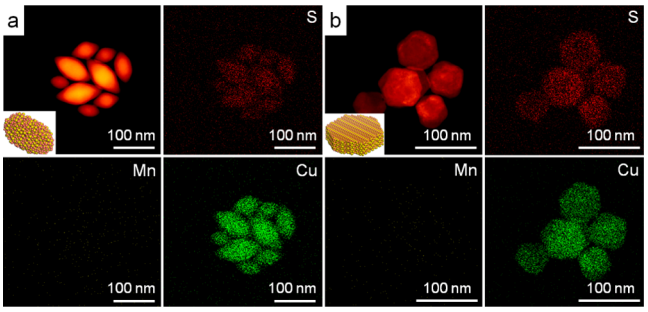

Figure 2. STEM-EDS elemental mapping images of (a) the monoclinic egg-like $Cu_{1.94}S$ nanocrystals and (b) the hexagonal CuS nanoplates (inset a and b are the corresponding crystal structures of the $Cu_{1.94}S$ nanocrystals and CuS nanoplates. Red ball represents Cu atom and yellow for S atom).

reaction processed for 10−15 min, as the color of the solution changed from brown to dark green, the egg-like nanocrystals grew into dumbbell-like architectures as mentioned above. Further increasing the reaction time to about 60 min, the middle parts of the structures disappeared and hexagonal CuS nanoplates (Figure S3) formed finally. However, the elemental Mn did not exist in the nanoplates (Figure 2b) either.

Previous findings proved that certain metal ion precursors played crucial role in controlling the morphology of nanostructures. For example, Cabot et al. and Pan et al. manipulated the formation of Cu_3Se_2 nanocubes and CuSe nanosheets with the assistance of Al^{3+} ions due to its promoting crystal growth in specific direction or combining with certain ions to regulate the nucleation and growth rate of another phase.[32,33] So we did a series of control experiments under the same conditions except for using other precursors. When $Zn(S_2CNEt_2)_2$ used, dumbbell-like ZnS-$Cu_{1.94}S$ heterostructures were obtained, as shown in Figure S4, consisting with our previous study.[34] Using $Cd(S_2CNEt_2)_2$ instead, according to the TEM images of Figure 3a, CdS-Cu_7S_4 heterostructures were

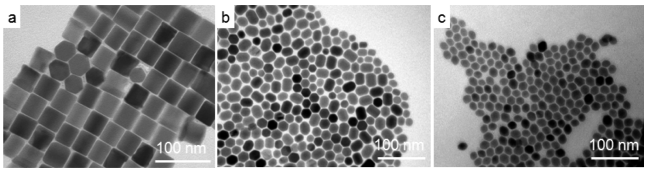

Figure 3. TEM images of the products (a) using $Cd(S_2CNEt_2)_2$, (b) using $Ni(S_2CNEt_2)_2$, and (c) using $Cu(S_2CNEt_2)_2$ instead of $Mn(S_2CNEt_2)_2$.

prepared, which was further confirmed by XRD and STEM-EDS elemental mapping analysis (Figure S5 and S6). If $Ni(S_2CNEt_2)_2$ or $Cu(S_2CNEt_2)_2$ used, we could only get $Cu_{1.94}S$ nanocrystals according to the characterization of TEM images (Figure 3b and 3c) and XRD patterns (Figure S7 and S8). On the basis of the experimental results above, it is evident that $Cu_{1.94}S$ nanocrystals are the sole products at the beginning of every experiment and only the manganous precursor can produce self-coupled $Cu_{2-x}S$ polymorphs. At the same time, we also explored the influence of halide ions on our experiment. As shown in Figure 4a, 4b and 4c, when CuBr used, we could also get egg-like nanocrystals, self-coupled polymorphs, and nanoplates similar to that of CuCl. As for CuI used, according to Figure 4d, 4e and 4f, we got nanofloriated crystals first, but they transformed to the self-coupled polymorphs and nanoplates

DOI: 10.1021/jacs.6b06609
J. Am. Chem. Soc. 2016, 138, 12913−12919

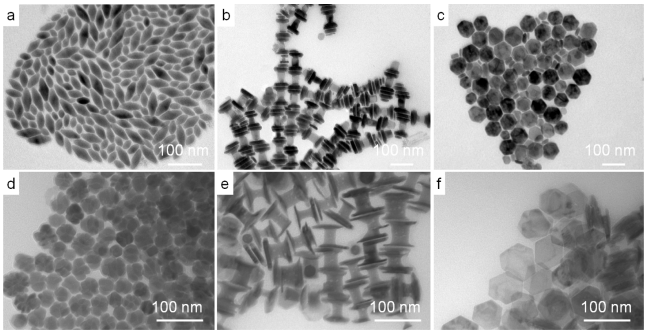

Figure 4. TEM images of the (a) $Cu_{1.94}S$ nanocrystals, (b) self-coupled $Cu_{1.94}S$-CuS polymorphs, (c) CuS nanoplates using CuBr instead of CuCl; (d, e, f) are the corresponding products using CuI instead.

eventually. Therefore, we could all get similar phase transformation and shape evolution process using different cuprous precursors. Thus, it can be conclusively presumed that it is the manganous precursor that mediates the whole conversion process from monoclinic $Cu_{1.94}S$ nanocrystals to hexagonal CuS nanoplates.

To theoretically examine the effect of the manganous precursor, we employed density functional calculation (DFT, see Experimental Section and Supporting Information for computational details) to calculate the binding energies between metal ions and ligands ($-S_2CNEt_2$). Obviously, according to Table S1, $Cu(S_2CNEt_2)$ is the least stable and Cu^+ ions are prior to reacting with ligands in the medium, then $Cu_{1.94}S$ were formed initially via decomposition. In addition, the lowest crystallization temperature of $Cu_{1.94}S$ is also a key factor for this occurrence. As for $Cd(S_2CNEt_2)_2$ or $Zn(S_2CNEt_2)_2$, Cd^{2+} or Zn^{2+} ions are comparable reactive and can partially compete with Cu^+ ions through cation exchange, thus ZnS/CdS-$Cu_{2-x}S$ were formed after generation of $Cu_{1.94}S$, while Cu^{2+} or Ni^{2+} ions are not favorable to react as the $Cu(S_2CNEt_2)_2$ or $Ni(S_2CNEt_2)_2$ are relatively stable and only $Cu_{1.94}S$ were obtained, which was in agreement with our experimental observations.

Thus, we propose the underlying mechanism as shown in Scheme S1: $Mn(S_2CNEt_2)_2$ has the most suitable binding energy (marked by a red circle in Table S2) between Mn^{2+} ions and ligands for appropriate cation exchange with Cu^+ ions and control the decomposition to $Cu_{1.94}S$ nanocrystals. Detailed thermal decomposition pathway is illustrated in reaction (1).[35] Besides $Cu_{1.94}S$, tetraethylthiourea ($SCN_2C_8H_{20}$) and carbon disulfide (CS_2) were formed as secondary sulfur sources, especially CS_2.[36] According to reaction (2) and (3), it can in situ generate H_2S and S_8 free radicals as active ingredients[37] and further react with oleylamine solvent to form thioamides and alkylammonium polysulfides as intermediate reactants in line with reaction (4), which has been deeply studied by Ozin et al.[38] Compared with Cu_2S, monoclinic $Cu_{1.94}S$ has more cationic vacancies, thus with high cationic mobility.[39] $Cu_{1.94}S$ nanocrystals then react with aforementioned sulfur species to form CuS nanoplates (reaction (5)). To verify this speculation, we separated the self-coupled polymorphs from the reaction medium to a fresh oleylamine system. As the former transformation (from $Cu_{1.94}S$ to $Cu_{1.94}S$-CuS) is too fast happening in just a few seconds, we could only explore the latter one (transformation from $Cu_{1.94}S$-CuS to CuS). We note that the shape and phase evolution does not occur under this condition, meaning this transformation process needs active species to motivate. However, if a trace amount of sulfur powder is added, the reaction happens rapidly to form CuS nanoplates (Figure S9), which is in accordance with what we propose in reaction (5). Additionally, Pradhan et al. discovered that Mn^{2+} ions could insert or eject from the structure causing reversible phase transformation by controlling atomic diffusion.[40] On account of this view, we hold that Mn^{2+} ions mediate the Cu^+ ions diffusion and phase conversion process particularly, as shown in Scheme 1. First Cu^+ ions at both tips

Scheme 1. Synthetic Pathway for Preparation of $Cu_{1.94}S$ Nanocrystals, Self-Coupled $Cu_{2-x}S$ Polymorphs and CuS Nanoplates Mediated by the Manganous Precursor

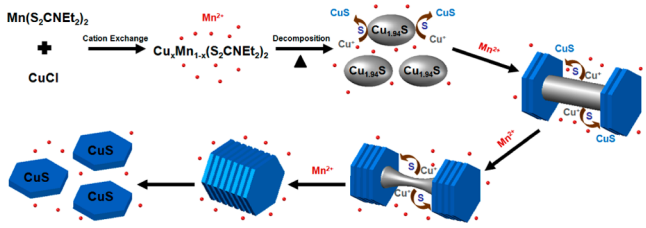

of the egg-like $Cu_{1.94}S$ nanocrystals were preferable to reacting with sulfur species to form CuS nanoplates because the tips of the $Cu_{1.94}S$ nanocrystals mainly exposed two sets of high-index facets ((731) and (804)) with high reactivity. The formed CuS nanoplates would stabilize the tips of the $Cu_{1.94}S$ and more orientational and stable facets between $Cu_{1.94}S$ and CuS were retained. Then the transformation process transferred to the middle part due to its full exposure to Mn^{2+} ions, as shown in Figure S10. It is obvious that $Cu_{1.94}S$ as the dumbbell handle was slowly consumed and the pure CuS nanoplates would form eventually. Similarly, we did an experiment in the same situation except for the absence of Mn^{2+} ions. Without Mn^{2+} ions, we could only get the CuS nanoplates with relatively smaller size rather than the self-coupled polymorphs when the color changed from brown to dark green immediately (Figure S11). This further convinces that Mn^{2+} ions could retard the phase transformation and shape evolution process from $Cu_{1.94}S$ nanocrystals to self-coupled $Cu_{2-x}S$ polymorphs.

Furthermore, we carried out XPS analysis to investigate the valency evolution of Cu and S during the whole process. As for Cu, the oxidation state was basically +1 with little change during the whole transformation process according to Figure 5a. While for S, several interesting changes were observed (Figure 5b), which was described in detail by deconvolution in subcomponents (Figure S12). It is composed of two doublet peaks, one is sulfide, changing from 161.5 to 161.0 eV due to the decrease of average length of Cu−S bond, the other is disulfide, emerging at 161.9 eV, which is the characteristic of S−S bond.[41] So the XPS changes well illustrated the phase transformation from $Cu_{1.94}S$ to CuS. Lately Manna et al. and Zhang et al. have both achieved the conversion from CuS to Cu_2S using a Cu (I) complex while maintaining the previous framework of the CuS nanoplates.[24,26] However, realizing the inverse process is rather challenging as lacking an appropriate "redox regulator". As far all we know, this is the first report on the successful evolution from Cu_2S to CuS that transforming from one with low density of free carriers and poor LSPR to a metallic and strongly plasmonic material mediated by a manganous precursor. Thus, we believe our finding may pave

DOI: 10.1021/jacs.6b06609
J. Am. Chem. Soc. 2016, 138, 12913−12919

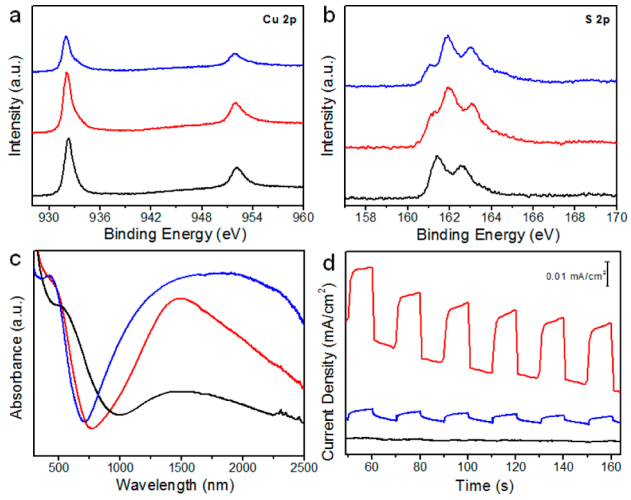

Figure 5. XPS spectra of (a) Cu 2p region and (b) S 2p region, (c) UV−vis−NIR absorption spectra, (d) photocurrent response of the $Cu_{1.94}S$ nanocrystals (black line), self-coupled $Cu_{2-x}S$ polymorphs (red line) and CuS nanoplates (blue line).

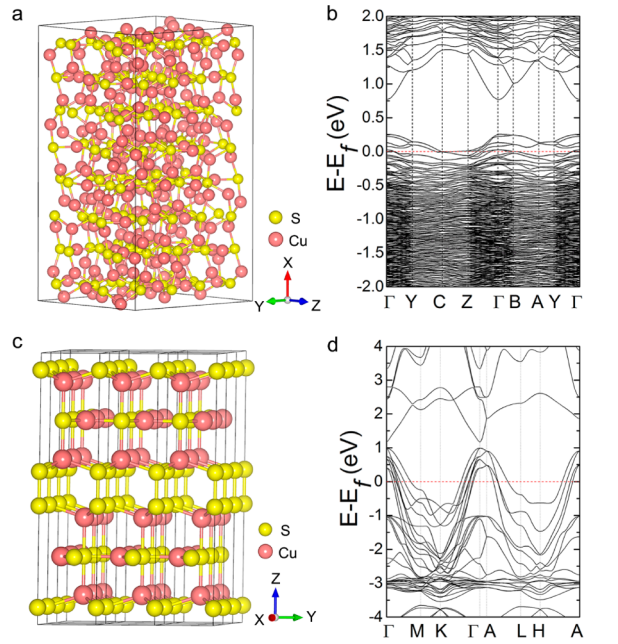

Figure 6. (a), (c) are the atomic arrangement representations and (b), (d) are the GGA + U band structures of $Cu_{1.94}S$ and CuS. Fermi levels are set to zero and marked as red dash lines. The high-symmetry points in Brillouin zone of $Cu_{1.94}S$ are Γ(0, 0, 0), Y(0,1/2,0), C(0, 1/2, 1/2), Z(0, 0, 1/2), B(−1/2, 0, 0) and A(−1/2, 1/2, 0), where those of CuS are Γ(0, 0, 0), M(0, 1/2, 0), K(−1/3, 2/3, 0), A(0, 0, 1/2), L(0, 1/2, 1/2) and H(−1/3, 2/3, 1/2).

the way to a novel family of chemical transformation and bring researchers to a deep understanding of the delicate details inside.

The optical absorption spectra of the different obtained nanostructures show significant absorbance across the solar spectrum and a broad near-infrared (NIR) absorption between 800 and 2500 nm (Figure 5c). Using the direct band gap method,[42] as shown in Figure S13, the band gaps of $Cu_{1.94}S$ and CuS are estimated to be 1.07 and 1.57 eV, which are rather suitable for photovoltaic and optoelectronic applications. The broad NIR absorption shown in spectra is derived from the intraband absorbance of free carries, more specifically of holes associated with the presence of Cu vacancies.[43,44] To elucidate the origin of the optical properties of $Cu_{1.94}S$ and CuS, DFT calculations were performed to analyze their electronic structures. As for $Cu_{1.94}S$ nanocrystals (Figure 6a), its Fermi level is 0.26 eV below the valence band maximum (VBM) under the impact of Mossec-Burstein effect[45] and the optical band gap between Fermi level and the conduction band minimum (CBM) is 0.77 eV (Figure 6b). In the case of CuS nanoplates (Figure 6c), GGA + U calculation shows the Fermi level is 0.99 eV below the VBM and the theoretical optical band gap is 1.18 eV (Figure 6d). Although GGA + U calculation underestimates the band gaps, it gives reasonable results of their electronic structures, which are consistent with results of HSE06 calculation (Figure S15). Typically, CuS with the Fermi level 0.99 eV below the VBM, which is much larger than the case in $Cu_{1.94}S$, even shows a metallic behavior of electrical transport due to the high density of charge carriers.[46]

To evaluate the potential of the self-coupled polymorphs for optoelectronic applications, we performed photoelectrochemical measurement using a three-electrode system comprising the sample film on the FTO as the working electrode, a Pt-coil counter electrode and a Ag/AgCl reference electrode. Figure 5d shows the time-dependent photoresponse of the three products at a constant bias voltage of −0.8 V (vs Ag/AgCl) and at the light-on and light-off time of 10 s. Under the same condition, we can see that among all the three samples, self-coupled $Cu_{2-x}S$ polymorphs exhibit the best photoresponse properties with the light current density of 0.12 mA/cm^2 (Figure S14). It means that the self-coupled polymorphs have superior charge separation and transport than individual $Cu_{1.94}S$ nanocrystals and CuS nanoplates under light irradiation.

In terms of the electronic structures of the $Cu_{1.94}S$ (100)-CuS (100) interfaces, potential analysis (Figure S16 and S17) show that the work function of $Cu_{1.94}S$(100) (ca. 4.56 eV) is lower than that of CuS(100) (ca. 5.24 eV), which suggests that the electrons flow from $Cu_{1.94}S$ to CuS. This is also supported by their differential charge density, $\Delta\rho = \rho(Cu_{1.94}S\text{-CuS}) - \rho(Cu_{1.94}S) - \rho(CuS)$ (Figure S18). The differential charge density analysis demonstrate that the charge transfer from $Cu_{1.94}S$ to CuS is 1.2 electrons, namely, about 6.0×10^{-3} e/Å^2 at the interface. The partial density of states (PDOS) and simulated charge distributions of the interface were shown in Figure 7a and 7b, and its band alignment from the PDOS is of an emerging type II, realizing the electron−hole separation in such heterointerfaces. According to Figure 7c, when two phases acquire an equalized Fermi level after contact, a potential difference from $Cu_{1.94}S$ to the CuS will be established. Meanwhile, the energy bands of $Cu_{1.94}S$ will shift downward, while the energy bands of CuS (100) will shift upward. Consequently, the CBM of $Cu_{1.94}S$ will become lower than that of CuS. As CuS and $Cu_{1.94}S$ absorb photons, the valence electrons will be excited to the CB and will leave holes in the VB. The photogenerated electrons produced by CuS will be injected into the CB of $Cu_{1.94}S$. Moreover, the photogenerated holes are effectively collected in the VB of CuS due to the contact potential difference, and readily transferred to working electrode due to the unique structure of the self-coupled polymorphs, which shows a strong anisotropic 2D character with better conductivity along the hexagonal planes, forming an emerging junction transporting holes. Thus, it can be greatly enhanced in dumbbell-like architecture due to the better contact of highly conductive hexagonal planes of CuS to the

DOI: 10.1021/jacs.6b06609
J. Am. Chem. Soc. 2016, 138, 12913−12919

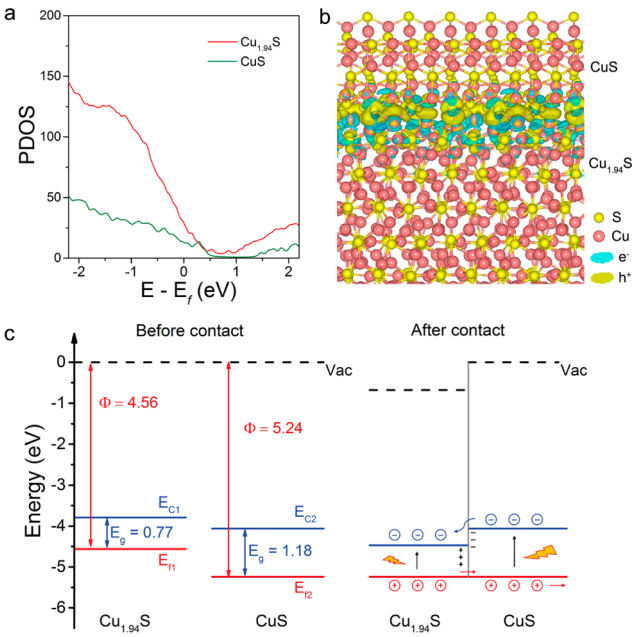

Figure 7. (a) Calculated partial density of states (PDOS) for the $Cu_{1.94}S$ (100) and CuS (100) fragments of the heterojunction. (b) Simulated charge distributions at the $Cu_{1.94}S$ (100)-CuS (100) heterojunction interface. (c) Schematic illustration of the band alignment and charge separation at the interface of the self-coupled $Cu_{2-x}S$ polymorphs. Φ, Vac, E_C, E_f are the work function, vacuum level, conduction band minimum, Fermi level, respectively. E_g is the optical band gap between the conduction band minimum and Fermi level.

electrode, thereby promoting the flow of photogenerated holes. Therefore, the probability of electron−hole recombination was reduced. Taking electronic structures and geometric configurations into account, the photoresponse property of the self-coupled polymorphs was significantly enhanced compared with the individuals.

CONCLUSIONS

In summary, unique self-coupled $Cu_{2-x}S$ polymorphs ($Cu_{1.94}S$-CuS) with dumbbell-like architecture were synthesized for the first time by the regulation of a manganous precursor. The self-coupled polymorphs can be isolated as the intermediate products of the phase transformation and shape evolution process from monoclinic $Cu_{1.94}S$ nanocrystals to hexagonal CuS nanoplates by controlling the reaction time. In addition, the self-coupled polymorphs as an emerging charge separation junction exhibit enhanced photoelectrochemical property compared with individual $Cu_{1.94}S$ nanocrystals and CuS nanoplates. As such, this colloidal method may provide a new avenue for controllable synthesis of a family of metal chalcogenide heteronanostructures and novel insights into the rational tuning of nanostructures with unique properties for application in optoelectronic devices or photocatalysis.

EXPERIMENTAL SECTION

Chemicals. The chemicals sodium diethyldithiocarbamate ($Na(S_2CNEt_2)$), $MnSO_4·4H_2O$, $ZnSO_4·7H_2O$, $CdCl_2·2.5H_2O$, $CuCl_2·4H_2O$, $NiCl_2·6H_2O$, CuCl, CuBr and CuI were purchased from Shanghai Reagent Company (P. R. China). Oleylamine (OLA, 70%) was purchased from Sigma-Aldrich. All chemicals were used as received without further purification.

Synthesis of $Mn(S_2CNEt_2)_2$ and Other Precursors. In a typical reaction for $Mn(S_2CNEt_2)_2$, $Na(S_2CNEt_2)$ (3 g) was dissolved in 100 mL distilled water (Solution 1) and $MnSO_4·4H_2O$ (3 g) was dissolved in 50 mL distilled water (Solution 2), respectively. Then Solution 2 was added into Solution 1 in a 250 mL beaker under stirring for 1 h. Finally the resulting dark brown precipitate was centrifuged (2000 rpm, 5 min), washed five times with distilled water, and dried under vacuum at 60 °C. As for $Zn(S_2CNEt_2)_2$, $Cd(S_2CNEt_2)_2$, $Cu(S_2CNEt_2)_2$ and $Ni(S_2CNEt_2)_2$, $ZnSO_4·7H_2O$, $CdCl_2·2.5H_2O$, $CuCl_2·4H_2O$ and $NiCl_2·6H_2O$ were used instead of $MnSO_4·4H_2O$.

Synthesis of the Self-Coupled $Cu_{2-x}S$ Polymorphs and Other Structures. In a typical procedure for the self-coupled $Cu_{2-x}S$ polymorphs, CuCl (0.015 g) (CuBr 0.02 g, CuI 0.025 g), $Mn(S_2CNEt_2)_2$ (0.025 g) and 5 mL OLA were mixed together in a 25 mL three-necked flask, and degassed under vacuum for 20 min. Then the reaction solution was heated under nitrogen to 125 °C at a rate of 10 °C/min, and kept for about 15 min (CuBr 10 min, CuI 3−5 min) and stopped when the color of the solution changed from brown to dark green. As for $Cu_{1.94}S$ nanocrystals, the reaction time was about 10 min (CuBr 7 min, CuI 1 min). As for hexagonal CuS nanoplates, the reaction time was about 60 min (CuBr 30 min, CuI 10 min). Lastly the obtained product was collected by centrifugation (8000 rpm, 3 min) and washed three times with hexane and ethanol for further characterization.

Instrumentation. The product was characterized by X-ray power diffraction (XRD), using a Philips X'Pert PRO SUPER X-ray diffractometer equipped with graphite monochromaticized Cu K radiation (λ = 1.54056 Å). The operation voltage and current were kept at 40 kV and 400 mA, respectively. TEM and HRTEM were performed on Hitachi H-7650 and JEOL-F2010 with an acceleration voltage of 200 kV respectively. HAADF-STEM and STEM EDS element mapping was carried out on Oxford Inca equipped on JEOL-F2010. Optical absorption spectra of samples dispersed in tetrachloroethylene were measured at room temperature using a DUV−3700 UV−vis−NIR spectrometer (Shimadzu).

Photoelectrochemical Measurement. Samples were coated on the FTO electrodes as follows: the products were dispersed in toluene with a concentration of 2.5 mg/mL, then 2 mL of the solution were spindropped on the 1.5 × 2 cm^2 FTO electrodes at 1500 r.p.m. for 30s by a desktop spin coater. After that the FTO electrodes were annealed at 450 °C for 1 h under Ar−H_2 gas mixture. The electrodes were immerged in 0.5 M Na_2SO_4 electrolyte. Current−time curves were acquired by an electrochemical analyzer system, Auto Lab workstation (PGSTAT302A) in a three-compartment cell with a working electrode, a platinum plate counter electrode, and a Ag/AgCl reference electrode under a bias voltage of −0.8 V using the excitation light of a 150 W Halogen lamp (DOLAN JENNER Model 150 Illuminator) as the light source.

DFT Calculations. Density-functional theory was applied to optimize geometries of free ligands, metal ions and their complexes in the Gaussian09 software.[47] B3LYP/genecp level of theory[48,49] was used with Lanl2dz basis set chosen for transition metal ions and 6-31g (d) for C, H, N, S atoms, respectively. SMD model was used to simulate the solvation effect[50] of oleylamine. All SMD computations were conducted at T = 298.15 K. SMD runs were all single point calculations with geometry optimizations in the gas phase. The binding energy is calculated as follows:

$$\Delta E_{BE} = E_{total} - E_{ion} - E_{ligand}$$

where ΔE_{BE} is the difference between electronic energy of the complex and components (metal ions and free ligands), while E_{ion}, E_{ligand} and E_{total} are the energy of the free metal ions, ligands and their complex, respectively. The Vienna ab initio simulation package (VASP)[51] with plane-wave basis set was used for geometry optimizations and electronic structure calculations of the interface. The projector augmented wave (PAW) method[52] in conjunction with a generalized gradient approximation (GGA)[53] of exchange-correlation functional in the PBE form[54] were adopted. A plane-wave cutoff of 400 eV was used for all calculations. The energy and residual force convergence criterion were set to 10^{-5} eV and 0.01 eV/Å for geometry, respectively.

DOI: 10.1021/jacs.6b06609
J. Am. Chem. Soc. 2016, 138, 12913−12919

The spin-polarized calculations were tested for CuS and $Cu_{1.94}S$, both found the nonspin-polarized states were the ground state. A Hubbard correction term[55] for the 3d electrons of copper was applied to the PBE calculation (DFT + *U*).[56] GGA + *U* calculations were performed in the simplified rotationally invariant approach, and the values of the exchange term *J* and coulomb term *U* were kept at 1.00 and 6.00 eV in all of the calculations.[57] The more details for $Cu_{1.94}S$-CuS model-building, band structures, surface potential diagram, differential charge density analysis and relevant references are provided in the Supporting Information.

■ ASSOCIATED CONTENT

Supporting Information

The Supporting Information is available free of charge on the ACS Publications website at DOI: 10.1021/jacs.6b06609.

Supporting tables, figures, schemes, and DFT calculations (PDF)

■ AUTHOR INFORMATION

Corresponding Authors

*shyu@ustc.edu.cn

*zyli@ustc.edu.cn

Author Contributions

‖S.-K.H., C.G., and S.Z. contributed equally to this work.

Notes

The authors declare no competing financial interest.

■ ACKNOWLEDGMENTS

We acknowledge the funding support from the National Natural Science Foundation of China (21431006, 21573201), the Foundation for Innovative Research Groups of the National Natural Science Foundation of China (21421063, 21521001), the National Basic Research Program of China (2014CB931800, 2013CB931800), the Users with Excellence and Scientific Research Grant of Hefei Science Center of CAS (2015HSC-UE007, 2015SRG-HSC038), the Chinese Academy of Sciences (KJZD-EW-M01-1, XDB01020300) and the China Postdoctoral Science Foundation (2013M540522).

■ REFERENCES

(1) Lesnyak, V.; Gaponik, N.; Eychmuller, A. *Chem. Soc. Rev.* **2013**, *42*, 2905.

(2) Talapin, D. V.; Lee, J. S.; Kovalenko, M. V.; Shevchenko, E. V. *Chem. Rev.* **2010**, *110*, 389.

(3) Wang, X.; Ren, X.; Kahen, K.; Hahn, M. A.; Rajeswaran, M.; Maccagnano-Zacher, S.; Silcox, J.; Cragg, G. E.; Efros, A. L.; Krauss, T. D. *Nature* **2009**, *459*, 686.

(4) Zhang, J.; Tang, Y.; Lee, K.; Ouyang, M. *Science* **2010**, *327*, 1634.

(5) Cortie, M. B.; McDonagh, A. M. *Chem. Rev.* **2011**, *111*, 3713.

(6) de Mello Donega, C. *Chem. Soc. Rev.* **2011**, *40*, 1512.

(7) Wu, X. J.; Chen, J.; Tan, C.; Zhu, Y.; Han, Y.; Zhang, H. *Nat. Chem.* **2016**, *8*, 470.

(8) Chen, J.; Wu, X. J.; Yin, L.; Li, B.; Hong, X.; Fan, Z.; Chen, B.; Xue, C.; Zhang, H. *Angew. Chem., Int. Ed.* **2015**, *54*, 1210.

(9) Vaneski, A.; Susha, A. S.; Rodriguez-Fernandez, J.; Berr, M.; Jackel, F.; Feldmann, J.; Rogach, A. L. *Adv. Funct. Mater.* **2011**, *21*, 1547.

(10) Li, P.; Wei, Z.; Wu, T.; Peng, Q.; Li, Y. *J. Am. Chem. Soc.* **2011**, *133*, 5660.

(11) Buck, M. R.; Bondi, J. F.; Schaak, R. E. *Nat. Chem.* **2012**, *4*, 37.

(12) Peng, S.; Lei, C.; Ren, Y.; Cook, R. E.; Sun, Y. *Angew. Chem., Int. Ed.* **2011**, *50*, 3158.

(13) Sun, X.; Guo, S.; Liu, Y.; Sun, S. *Nano Lett.* **2012**, *12*, 4859.

(14) Habas, S. E.; Yang, P.; Mokari, T. *J. Am. Chem. Soc.* **2008**, *130*, 3294.

(15) Zhuang, T. T.; Liu, Y.; Sun, M.; Jiang, S. L.; Zhang, M. W.; Wang, X. C.; Zhang, Q.; Jiang, J.; Yu, S. H. *Angew. Chem., Int. Ed.* **2015**, *54*, 11495.

(16) Han, S. K.; Gu, C.; Gong, M.; Yu, S. H. *J. Am. Chem. Soc.* **2015**, *137*, 5390.

(17) Tan, C.; Zeng, Z.; Huang, X.; Rui, X.; Wu, X. J.; Li, B.; Luo, Z.; Chen, J.; Chen, B.; Yan, Q.; Zhang, H. *Angew. Chem., Int. Ed.* **2015**, *54*, 1841.

(18) Luther, J. M.; Jain, P. K.; Ewers, T.; Alivisatos, A. P. *Nat. Mater.* **2011**, *10*, 361.

(19) Han, W.; Yi, L.; Zhao, N.; Tang, A.; Gao, M.; Tang, Z. *J. Am. Chem. Soc.* **2008**, *130*, 13152.

(20) Larsen, T. H.; Sigman, M.; Ghezelbash, A.; Doty, R. C.; Korgel, B. A. *J. Am. Chem. Soc.* **2003**, *125*, 5638.

(21) Sigman, M. B., Jr.; Ghezelbash, A.; Hanrath, T.; Saunders, A. E.; Lee, F.; Korgel, B. A. *J. Am. Chem. Soc.* **2003**, *125*, 16050.

(22) Zhuang, Z.; Peng, Q.; Zhang, B.; Li, Y. *J. Am. Chem. Soc.* **2008**, *130*, 10482.

(23) Ma, G.; Zhou, Y.; Li, X.; Sun, K.; Liu, S.; Hu, J.; Kotov, N. A. *ACS Nano* **2013**, *7*, 9010.

(24) Bryks, W.; Wette, M.; Velez, N.; Hsu, S. W.; Tao, A. R. *J. Am. Chem. Soc.* **2014**, *136*, 6175.

(25) Du, Y.; Yin, Z.; Zhu, J.; Huang, X.; Wu, X. J.; Zeng, Z.; Yan, Q.; Zhang, H. *Nat. Commun.* **2012**, *3*, 1177.

(26) Wu, X. J.; Huang, X.; Liu, J.; Li, H.; Yang, J.; Li, B.; Huang, W.; Zhang, H. *Angew. Chem., Int. Ed.* **2014**, *53*, 5083.

(27) Xie, Y.; Carbone, L.; Nobile, C.; Grillo, V.; D'Agostino, S.; Della Sala, F.; Giannini, C.; Altamura, D.; Oelsner, C.; Kryschi, C.; Cozzoli, P. D. *ACS Nano* **2013**, *7*, 7352.

(28) Xie, Y.; Riedinger, A.; Prato, M.; Casu, A.; Genovese, A.; Guardia, P.; Sottini, S.; Sangregorio, C.; Miszta, K.; Ghosh, S.; Pellegrino, T.; Manna, L. *J. Am. Chem. Soc.* **2013**, *135*, 17630.

(29) Liu, M. X.; Xue, X. Z.; Ghosh, C.; Liu, X.; Liu, Y.; Furlani, E. P.; Swihart, M. T.; Prasad, P. N. *Chem. Mater.* **2015**, *27*, 2584.

(30) Hsu, S. W.; Ngo, C.; Bryks, W.; Tao, A. R. *Chem. Mater.* **2015**, *27*, 4957.

(31) Wu, X. J.; Huang, X.; Qi, X.; Li, H.; Li, B.; Zhang, H. *Angew. Chem., Int. Ed.* **2014**, *53*, 8929.

(32) Li, W.; Zamani, R.; Ibanez, M.; Cadavid, D.; Shavel, A.; Morante, J. R.; Arbiol, J.; Cabot, A. *J. Am. Chem. Soc.* **2013**, *135*, 4664.

(33) Liu, Y. Q.; Wu, H. D.; Zhao, Y.; Pan, G. B. *Langmuir* **2015**, *31*, 4958.

(34) Han, S. K.; Gong, M.; Yao, H. B.; Wang, Z. M.; Yu, S. H. *Angew. Chem., Int. Ed.* **2012**, *51*, 6365.

(35) Jen-La Plante, I.; Zeid, T. W.; Yang, P.; Mokari, T. *J. Mater. Chem.* **2010**, *20*, 6612.

(36) Mahler, B.; Hoepfner, V.; Liao, K.; Ozin, G. A. *J. Am. Chem. Soc.* **2014**, *136*, 14121.

(37) Ballabeni, M.; Ballini, R.; Bigi, F.; Maggi, R.; Parrini, M.; Predieri, G.; Sartori, G. *J. Org. Chem.* **1999**, *64*, 1029.

(38) Thomson, J. W.; Nagashima, K.; Macdonald, P. M.; Ozin, G. A. *J. Am. Chem. Soc.* **2011**, *133*, 5036.

(39) Zhu, G.; Xu, Z. *J. Am. Chem. Soc.* **2011**, *133*, 148.

(40) Karan, N. S.; Sarkar, S.; Sarma, D. D.; Kundu, P.; Ravishankar, N.; Pradhan, N. *J. Am. Chem. Soc.* **2011**, *133*, 1666.

(41) Fu, W.; Liu, L.; Yang, G.; Deng, L.; Zou, B.; Ruan, W.; Zhong, H. *Part. Part. Syst. Charact.* **2015**, *32*, 907.

(42) Han, S. K.; Gu, C.; Gong, M.; Wang, Z. M.; Yu, S. H. *Small* **2013**, *9*, 3765.

(43) Zhao, Y.; Pan, H.; Lou, Y.; Qiu, X.; Zhu, J.; Burda, C. *J. Am. Chem. Soc.* **2009**, *131*, 4253.

(44) Hsu, S. W.; On, K.; Tao, A. R. *J. Am. Chem. Soc.* **2011**, *133*, 19072.

(45) Lukashev, P.; Lambrecht, W. R.; Kotani, T.; Schilfgaarde, M. V. *Phys. Rev. B: Condens. Matter Mater. Phys.* **2007**, *76*, 195202.

(46) Casaca, A.; Lopes, E. B.; Gonçalves, A. P.; Almeida, M. *J. Phys.: Condens. Matter* **2012**, *24*, 015701.

(47) Frisch, M. J.; Trucks, G. W.; Schlegel, H. B.; Scuseria, G. E.; et al. *Gaussian 09*, Revision A.1; Gaussian, Inc.: Wallingford, CT, 2009.

(48) Becke, A. D. *J. Chem. Phys.* **1993**, *98*, 5648.
(49) Lee, C.; Yang, W.; Parr, R. G. *Phys. Rev. B: Condens. Matter Mater. Phys.* **1988**, *37*, 785.
(50) Marenich, A. V.; Cramer, C. J.; Truhlar, D. G. *J. Phys. Chem. B* **2009**, *113*, 6378.
(51) Kresse, G.; Furthmüller, J. *Phys. Rev. B: Condens. Matter Mater. Phys.* **1996**, *54*, 11169.
(52) Blöchl, P. E. *Phys. Rev. B: Condens. Matter Mater. Phys.* **1994**, *50*, 17953.
(53) Yang, W.; Parr, R. G. *Density-Functional Theory of Atoms and Molecules*; Oxford University Press, 1989.
(54) Perdew, J. P.; Burke, K.; Ernzerhof, M. *Phys. Rev. Lett.* **1996**, *77*, 3865.
(55) Hubbard, J. *Proc. R. Soc. London, Ser. A* **1963**, *276*, 238.
(56) Dudarev, S. L.; Botton, G. A.; Savrasov, S. Y.; Humphreys, C. J.; Sutton, A. P. *Phys. Rev. B: Condens. Matter Mater. Phys.* **1998**, *57*, 1505.
(57) Morales-García, A.; Soares, A. L., Jr; Dos Santos, E. C.; de Abreu, H. A.; Duarte, H. A. *J. Phys. Chem. A* **2014**, *118*, 5823.

DOI: 10.1021/jacs.6b06609
J. Am. Chem. Soc. 2016, 138, 12913−12919